CORRECTION

A Robust Design for Cellular Vehicles of Gold Nanorods for Multimodal Imaging

F. Ratto, S. Centi, C. Avigo, C. Borri, F. Tatini, L. Cavigli, C. Kusmic, B. Lelli, S. Lai, S. Colagrande, F. Faita, L. Menichetti, and R. Pini*

Adv. Funct. Mater. **2016**, *39*, 7178

DOI: 10.1002/adfm.201600836

Authors Dr. Marisa Benagiano and Prof. Mario Milco D'Elios were not included when this article was originally published. The corrected list of author of this manuscript is:

F. Ratto, S. Centi, C. Avigo, C. Borri, F. Tatini, L. Cavigli, C. Kusmic, B. Lelli, S. Lai, M. Benagiano, M. M. D'Elios, S. Colagrande, F. Faita, L. Menichetti, and R. Pini*

The affiliation for Dr. Benagiano and Prof. D'Elios is:

Department of Experimental and Clinical Medicine

University of Florence, Largo Brambilla 3, 50134 Florence, (FI), Italy

Ref. [82] was not included in the originally published version of this article. It should be added to the second paragraph on page 7179, which then reads as follows:

"More recently, the notion to exploit the natural tropism of cells, such as tumor-associated macrophages,[35–39] T cells,[40,82] mesenchymal stem cells,[41–43] and neural stem cells,[44,45] has begun to emerge as a radical alternative."

Ref. [82] is:

G. Baldi, C. Ravagli, M. Comes Franchini, M. M. D'Elios, M. Benagiano, M. Bitossi (Colorobbia Italia S.p.A.) *WO 104664*, **2015**.

The Acknowledgements should be corrected to read as follows:

"This work was in part supported by the Projects of Tuscan Region "NANOTREAT" and "SYNERGY" and by the ERANET+ Project of Tuscan Region and European Community "LUS BUBBLE". The authors wish to thank Dr. Daniele Panetta for his expertise in X-ray micro imaging and Dr. Giovanni Baldi of CERICOL Research Center of Colorobbia Group for his expertise and knowledge on cellular nano-engineering."

The authors apologize for any inconvenience or misunderstanding that these errors may have caused.

ADVANCED FUNCTIONAL MATERIALS
www.afm-journal.de

A Robust Design for Cellular Vehicles of Gold Nanorods for Multimodal Imaging

Fulvio Ratto, Sonia Centi, Cinzia Avigo, Claudia Borri, Francesca Tatini, Lucia Cavigli, Claudia Kusmic, Beatrice Lelli, Sarah Lai, Stefano Colagrande, Francesco Faita, Luca Menichetti, and Roberto Pini*

The pursuit of more selectivity in the delivery of plasmonic particles to tumors is critical before their penetration into clinical applications as the photoacoustic imaging and the photothermal ablation of cancer. As their direct infusion into the bloodstream remains problematic, due to a multitude of biological barriers, the development of alternative approaches is emerging as a new challenge. In this context, the recruitment of homologous tumor-tropic cells that may serve as Trojan horses stands out as a fascinating possibility. Here, a novel model of gold nanorods is presented that feature a composite shell and undergo efficient and reproducible endocytic uptake from murine macrophages, which is fine-tunable over a broad range of conditions. These cells preserve their viability and more than 90% of their innate chemotactic behavior in vitro, even with a cargo exceeding 200 000 particles per cell. In addition, we show that these vehicles are detectible by photoacoustic imaging down to concentrations in the order of 1% in whole blood and by clinical X-ray computed tomography below 10%, which is within the typical fraction of a leukocytic infiltrate in a tumor microenvironment, and may even work as contrast agents for the photothermal ablation of cancer.

1. Introduction

The clinical exploitation of plasmonic particles such as gold nanorods, shells, cages, and other nonspherical shapes has become a remarkable mission for a willful community of scientists.[1–6] These particles are being proposed as contrast agents for various applications in biomedical optics, including the photothermal ablation and the photoacoustic imaging (PAI)[7,8] of cancer, which are emerging as hopeful alternatives in oncology. A favorable premise of gold nanoparticles is their good tolerability in vivo.[9–11] Moreover, at variance with gold nanospheres that resonate in the green as many biological dyes including hemoglobin, the particular shapes of gold nanorods, shells, and cages originate new bands of optical absorbance in the near infrared (NIR),[12] which are ideal to achieve high penetration and contrast in biotissue. In particular, the plasmonic bands of gold nanorods are tunable across the entire window of the NIR with their size and shape and provide for unique cross sections of optical absorbance.[5,13–15] Their efficiency of photothermal conversion outclasses that of organic dyes by several orders of magnitude and also that of alternative gold nanoparticles.[16,17] Another advantage over organic dyes is the stability of these cross sections in biological fluids. However, new pitfalls are hidden at the interface with cells.[9] For instance, as gold nanoparticles undergo endocytic uptake, their aggregation within tight vesicles may jeopardize their optical features,[18–20] due to plasmonic coupling. Different authors have proposed the use of rigid shells such as silica as a spacer to prevent this warning.[19,21] Indeed, floccules of silanized gold nanorods in anhydrous biopolymers retain most of their optical features, while softer shells such as polyethylene glycol (PEG) are ineffective.[18] However, while inorganic shells may provide new functions,[22,23] we found a different scenario in endocytic vesicles. There, we noted that PEG strands of the appropriate weight are enough to inhibit plasmonic coupling.[24] In essence, whereas PEG shells collapse in anhydrous environments, their steric hindrance works well in moist conditions, even at extreme concentrations. In addition, the colloidal stability of PEGylated gold nanorods in biological fluids is critical for the feasibility of their tests in vitro and in vivo.[25,26]

At present, one of the most relevant challenges in nanomedicine is to really optimize the delivery of functional nanoparticles into tumors upon systemic administration, as a magic bullet. In this context, PEGylated gold nanorods are a promising platform.

Dr. F. Ratto, Dr. S. Centi, Dr. F. Tatini, Dr. L. Cavigli, B. Lelli, Dr. S. Lai, Dr. R. Pini
Institute of Applied Physics 'N. Carrara'
National Research Council Italy
via Madonna del Piano 10
50019 Sesto Fiorentino, (FI), Italy
E-mail: f.ratto@ifac.cnr.it
C. Avigo, Dr. C. Kusmic, Dr. F. Faita, Dr. L. Menichetti
Institute of Clinical Physiology
National Research Council Italy
via Moruzzi 1, 56124 Pisa, (PI), Italy
Dr. C. Borri, Prof. S. Colagrande
Department of Experimental and Clinical Biomedical Sciences 'M. Serio'
University of Florence
largo Brambilla 3, 50134 Florence, (FI), Italy

DOI: 10.1002/adfm.201600836

Their hydrodynamic size is ideal to passively pervade tumors that exhibit enhanced vascular permeability and poor lymphatic drainage.[10,27–29] Besides, PEG strands and other spacers holding reactive moieties enable their bioconjugation with targeting units that actively bind malignant phenotypes.[20,24,30,31] PEGylated and bioconjugated gold nanorods display high specificity and blood compatibility in vitro.[30] Therefore, their direct injection into the bloodstream has become a mainstream solution. However, after more than one decade of preclinical trials in dozens of labs, this route still remains problematic. Upon intravenous injection, more than ≈90% of the gold nanorods typically get captured by the mononuclear phagocyte system (MPS).[4,10,32,33] Indeed the complexity of the biological barriers in the body,[34] comprising the MPS, the vessel walls, the tumor stroma, etc. poses a formidable challenge to really optimize the design of these particles.

More recently, the notion to exploit the natural tropism of cells, such as tumor-associated macrophages,[35–39] T cells,[40] mesenchymal stem cells,[41–43] and neural stem cells,[44,45] has begun to emerge as a radical alternative. These cells hold an innate ability to detect and to infiltrate tumors with high specificity,[46–49] with the aim to modulate their microenvironment in a variety of ways. In particular, macrophagic infiltrates are common in cancer as well as in atherosclerosis, myocardial infarction, aortic aneurysm, diabetes, and other conditions and are emerging as a new target for imaging and treatments.[50–54] In most tumors, the extent of macrophagic infiltrates correlates with a poor prognosis and may exceed 50% of their size.[55–57] These macrophages accumulate even in hypoxic and necrotic segments, stimulate the angiogenesis, support the malignant cells in terms of invasion, motility, intravasation in primary sites and of extravasation, survival, and persistent growth in metastatic sites, prime premetastatic sites, and also play an immunosuppressive role, by protecting the malignant cells against natural killer and T cells.[47] In turn, tumor-associated macrophages may be conceived of as Trojan horses to take up and to deliver functional cargos to their biological target, including plasmonic particles such as gold nanoshells.[35–39] Several authors have suggested that this approach may improve the distribution and retention of different particles both in malignant against normal tissue[36,40,42] and within malignant tissue.[43–45] Other advantages include a full personalization of the treatment and a remarkable simplification of the biological interface.

In essence, the design of gold nanorods needs to provide for their efficient uptake from macrophagic cells that maintain their viability and tropism. Over recent years, Vigderman et al.[58] and Schnarr et al.[45] have shown that quaternary ammonium compounds are capable to drive a massive uptake of gold nanorods into endocytic vesicles, due to their positive zeta potential.[59] Here, we combine this notion with the observation that cell penetrating agents with a cationic profile[60,61] preserve their functionality after inclusion within PEG shells,[62] which add colloidal stability and biocompatibility.[25,26] We propose a novel design of polycationic gold nanorods that enable a robust fabrication of cellular vehicles. We demonstrate their viability and tropism and their use as contrast agents for PAI and X-ray computed tomography (CT) even in whole human blood in a tissue-like optical phantom down to concentrations of a few percent, which is at least an order of magnitude below the typical extent of macrophagic infiltrates in tumors. While previous work has demonstrated the use of cellular vehicles for specific applications in vivo,[36,40,42–44,46] our primary focus rests on an innovative design of plasmonic particles for an efficient integration into macrophages exhibiting functional optical features and maintaining their viability and chemotactic performance.

2. Results and Discussion

2.1. Polycationic Gold Nanorods

As it is discussed in the Experimental Section, gold nanorods were PEGylated and then saturated with (11-Mercaptoundecyl)-N,N,N-trimethylammonium bromide (MUTAB) in one pot, in order to achieve polycationic particles. Their zeta potential was (20 ± 2) mV, which is attributed to the permanent charge of the quaternary ammonium moieties of MUTAB. As a reference, this value dropped to (−18 ± 2) mV when MUTAB was replaced with 11-mercaptoundecanoic acid, which only differs from MUTAB by the substitution of the quaternary ammonium end with a C-terminus. The zeta potential of polycationic gold nanorods from different batches within a range of aspect ratios from ≈3.0 to ≈4.5 and effective radii around 10 nm was found to differ from each other by less than ±10%. The colloidal stability of these particles proved to be optimal even after at least five cycles of centrifugation and dispersion in phosphate buffered saline (PBS) and various culture media up to gold contents around 80×10^{-3} M Au, which is about the PEG shells. We note that, when we tried to modify gold nanorods with MUTAB in the absence of PEG, as in Schnarr et al.[45] and Mooney et al.[44] particles began to flocculate in PBS soon after the first cycle of centrifugation, which would be a major concern for the reproducibility of their applications.

2.2. Plasmonic Macrophages: Optical Features

Murine macrophages were incubated with different concentrations of polycationic gold nanorods over different times. **Figure 1** and Figure S1 of the Supporting Information report representative images of macrophages treated for 24 h with 400×10^{-6} M Au. The presence of a dark particulate within the perinuclear cytoplasm is already visible by the use of an optical microscope, as it is seen in Figure S1 of the Supporting Information. On closer inspection by the use of electron microscopy, gold nanorods are seen to undergo tight confinement within endocytic vesicles that exhibit a broad range of sizes in the order of a few hundred nm and distances of a few µm, which is consistent with the findings from other authors.[20,45,58,59]

On visual inspection, the pellets of these cells became darker and darker both with the increase of incubation dosage and time. In an attempt to quantify the underlying kinetics, these pellets were fixed, resuspended in PBS and directed to an optical analysis. Their spectra of optical extinction revealed the same plasmonic bands as the original suspensions of gold nanorods, with minimal modifications (see Figure S2, Supporting Information), which implies the absence of significant plasmonic coupling. Their lineshapes were modeled as the

Adv. Funct. Mater. 2016,
DOI: 10.1002/adfm.201600836

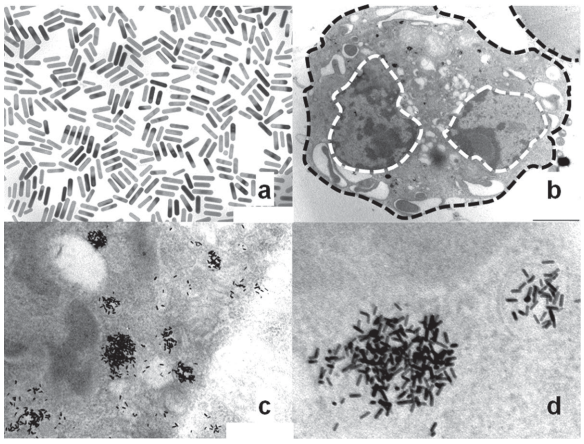

Figure 1. a) (650 × 500) nm^2 TEM image of assynthesized gold nanorods; b–d) (13 × 8.6) μm^2, (2.3 × 1.7) μm^2, and (870 × 650) nm^2 TEM images of macrophages grown on polycarbonate membranes and treated for 24 h with polycationic gold nanorods at a concentration of 400 × 10^{-6} M Au. In panel (b), black and white dotted lines, respectively, denote plasmatic and nuclear membranes. For sample preparation, macrophages were fixed, and included in an epoxidic resin with their polycarbonate substrate. The appearance of the particles in panel (d) is affected by their inclination in the endocytic vesicles.

sum of an empirical background from an unknown number of cells, which was calibrated in a preliminary measurement, plus a numerical approximation of the plasmonic band from an unknown number of gold nanorods. The latter was devised as a convolution integral between Gans lineshape,[15,63,64] which was implemented with the dielectric function by Etchegoin et al.[65] and an unknown distribution of aspect ratios. Details and a demonstration of this method are reported elsewhere.[24,63,64] The output of this analysis is a number of particles per cell. Results are displayed in **Figure 2**. The number of

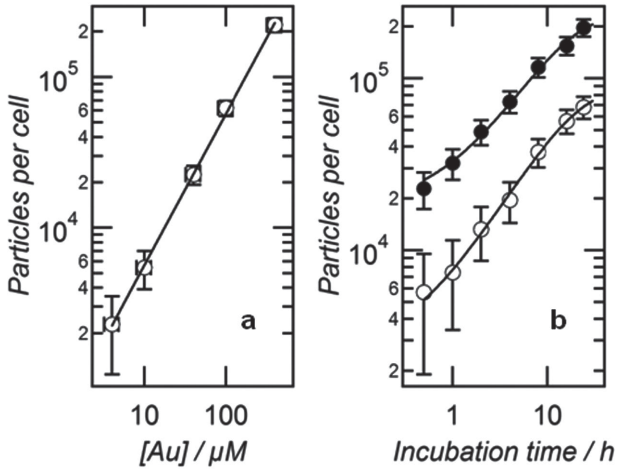

Figure 2. Number of polycationic gold nanorods that are taken up per macrophagic cell treated in a) for 24 h at different concentrations of gold and in b) for different incubation times with 100 × 10^{-6} (empty circles) and 400 × 10^{-6} M (full circles) Au. Data were retrieved from an optical analysis of aqueous suspensions of these cells and expressed as average ± standard deviation of three independent runs.

particles per cell is linear with incubation dosage and undergoes exponential saturation with incubation time. In particular, after 24 h, the effective rate of uptake per unit of incubation dosage is (580 ± 40) particles/cell/μM Au. In turn, with an incubation dosage of 400 × 10^{-6} M Au, the initial rate of uptake per unit of incubation time is (260 ± 50) particles/cell /min. In practice, macrophages treated for 24 h with 400 × 10^{-6} M Au contain as many as ≈200 000 gold nanorods. These figures are in the same order of magnitude as the records that were reported by Vigderman et al.[58] when it is considered that macrophages are smaller than other kinds of cells. However, at variance with the use of particles without PEG, where the uptake of gold was found to vary from replica to replica by as much as a factor of ≈3000%[44] under identical conditions, we verified that our protocol is reproducible within ±20%. This dramatic improvement is attributed to the colloidal stability that belongs to the steric hindrance of PEG. In addition, this hindrance persists even in the extreme densities of the endocytic vesicles, which is demonstrated by the near-absence of plasmonic coupling in the spectra of optical extinction in Figure S2 of the Supporting Information.

2.3. Plasmonic Macrophages: Viability and Tropism

Perhaps, the most critical concern for the preparation of cellular vehicles is about the preservation of their biological functions of interest. Both the optical and the electron images of our macrophages reveal that their morphology remains normal upon interaction with polycationic gold nanorods, which points to an overall conservation of their physiology.

Figure 3a displays the viability of these cells upon incubation with cationic gold nanorods. A modest decrease is seen both with the incubation dosage and time, which is more likely to result from a reduction of cell proliferation rather than the onset of apoptosis or necrosis, according to our optical images. After incubation for 24 h with 400 × 10^{-6} M Au, the viability is still within ≈10% of control. Therefore we conclude that no significant cytotoxic effect is detectible within the range of conditions that was explored.

Figure 3b shows the migration of macrophages treated with 100 × 10^{-6} and 400 × 10^{-6} M Au for 24 h with respect to controls in the presence and absence of a chemotactic stimulus, such as a gradient of MIP-1α.[66] We emphasize that these cells were first prepared with polycationic gold nanorods and then tested for their chemotactic migration, as it would occur in a real-world application. Also this parameter keeps satisfactory.

Blank cells exhibit a very low level of motility in serum-free medium without chemokine. Likewise, the treatment with gold nanorods alone does not trigger their chemotaxis, thus demonstrating that these particles are unable to activate murine macrophages. Conversely, their incubation with MIP-1α (50 ng mL^{-1}) exerts a sharp increase in their chemotaxis. More than 90% of this migration is still observed in macrophages that were pretreated with 100 × 10^{-6} and 400 × 10^{-6} M Au and then exposed to MIP-1α. Therefore, our polycationic gold nanorods do not inhibit the chemotaxis of murine macrophages under these conditions.

These results are in line with those by Schnarr et al.[45] and Madsen et al.[38] and suggest that the chemotactic functions

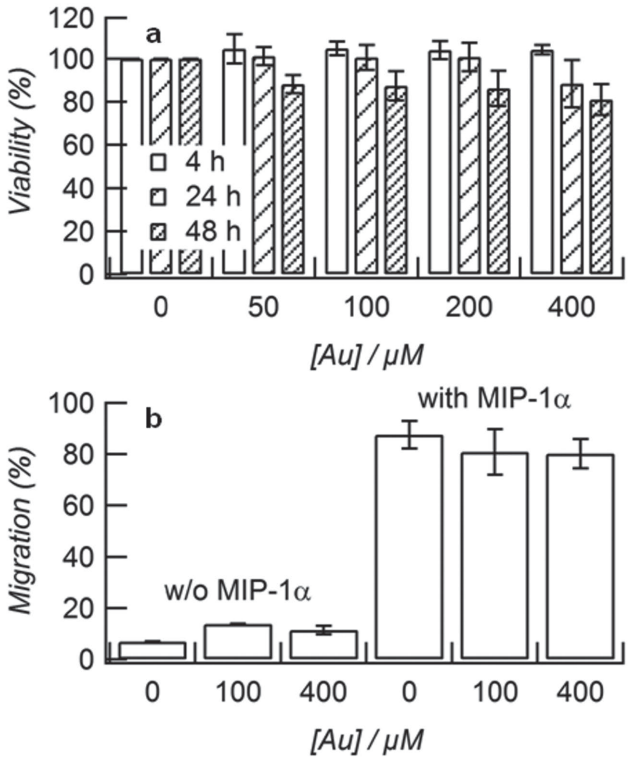

Figure 3. a) Viability of macrophagic cells treated for different incubation times with different concentrations of gold and retrieved from a WST-8 assay. Data are expressed as percent of formazan with respect to controls. Values are reported as mean ± SD of three independent experiments; b) percent of macrophages treated for 24 h with different concentrations of gold that migrated after exposure to MIP-1α with respect to controls. The chemotaxis assay was performed by the use of Transwell permeable membranes. Results are shown as mean ± SD of three independent experiments.

of macrophages are robust in the presence of nontoxic gold nanoparticles.

Overall, our macrophages maintain well their viability and tropism in vitro, which is their principal functions in view of their use as Trojan horses.

2.4. Plasmonic Macrophages: Contrast for Biomedical Imaging

The possibility to map macrophagic infiltrates of cells treated with polycationic gold nanorods was addressed by PAI. These cells are tested as exogenous agents to enhance the optical contrast by their plasmonic cargo and to break through the imaging-depth limit. With this approach, the excitation of the plasmonic oscillations of gold nanorods with short optical pulses triggers a cascade of photothermal and thermoelastic conversion in their fluid environment, which leads to the emission of ultrasound.[7,8] Here, we combined a high resolution photoacoustic and micro-ultrasound platform that operates in the range of wavelengths between 680 and 970 nm and a linear array transducer. As for the samples, we used a tissue-like optical phantom to achieve semiquantitative data from sets of microchannels drawn in a polymeric scaffold. Meanwhile, owing to the large atomic number of gold, we investigated the possibility to detect our macrophages with a microCT scanner.

The fingerprint of plasmonic macrophages was detected by the use of photoacoustic spectroscopy.[67,68] First, we recorded the photoacoustic signals from microchannels that were filled with aqueous suspensions of gold nanorods without cells. These data are reported in Figure S3 of the Supporting Information and reveal that the plasmonic bands of these samples are retraced well down to concentrations in the range of ≈100 × 10^{-6} M Au. The intensity of the photoacoustic signals undergoes exponential saturation with the dosage of gold, as the optical fluence becomes more and more exhausted by the particles, which was used to establish a calibration curve. Next, the microchannels were filled with ≈10^7 plasmonic macrophages per cc. In this case, the shape of the photoacoustic spectra departs a little further from that of the optical extinction, which we ascribe to the onset of nonlinear effects, such as cavitation,[68,69] that grow up in the extreme densities of the endocytic vesicles.[70,71] Nonetheless, the intensity of the photoacoustic signals still scales with the number of particles per cell and fits rather well in the calibration curve, when the data from Figure 2 are worked out into the overall content of gold in these samples. All these data demonstrate that macrophages treated for 24 h with 100 × 10^{-6} to 400 × 10^{-6} M Au are discriminated well from a background of PBS even at a concentration of ≈1% (v/v), which is at least an order of magnitude below the typical fraction of the macrophagic infiltrate in a malignant lesion.

The same applies to whole blood as well. **Figure 4**a,b shows photoacoustic spectra and a representative photoacoustic image of three microchannels that were filled with human whole blood, a suspension of gold nanorods in whole blood at the concentration of 1 × 10^{-3} M Au and whole blood containing ≈3% (v/v) macrophages treated for 24 h with 400 × 10^{-6} M Au. The photoacoustic spectra of whole blood display the typical fingerprint of oxygenated hemoglobin.[72,73] In addition to this fingerprint, the plasmonic band of gold nanorods dominates in both other samples and its intensity scales well with the concentration of gold, when it is considered that ≈3% (v/v) macrophages treated for 24 h with 400 × 10^{-6} M Au amounts to (2.3 ± 0.5) × 10^{-3} M Au. Figure 4a demonstrates that the detection limit of the plasmonic macrophages in whole blood falls well below 3% (v/v), which substantiates the feasibility of this approach in vivo.

In order to understand the possibility to image the accumulation of these cells even deeper inside biotissue, we verified the contrast of gold nanorods by conventional CT from relevant inclusions of a volume of ≈100 μL. Figure S4 of the Supporting Information displays our calibration curve. At variance with the previous work by von Maltzahn et al.[17] we focused on a regime of lower concentrations of gold, which may be accessible by the use of cellular vehicles. In this regime, upon optimization of the setup, the absorbance is linear with the concentration of Au with a rate of (16 ± 2) H.U./mM Au.

Figure 4c displays a CT image of a set of inclusions containing standard solutions of iodine in PBS, suspensions of gold nanorods in PBS at the concentration of 4 × 10^{-3} M Au, and ≈8% (v/v) macrophages treated for 24 h with 400 × 10^{-6} M Au. We note that the latter is still well below the possible content of tumor-associated macrophages in a malignant lesion. Therefore, the combination of Figure 4b,c illustrates the potential of

DOI: 10.1002/adfm.201600836

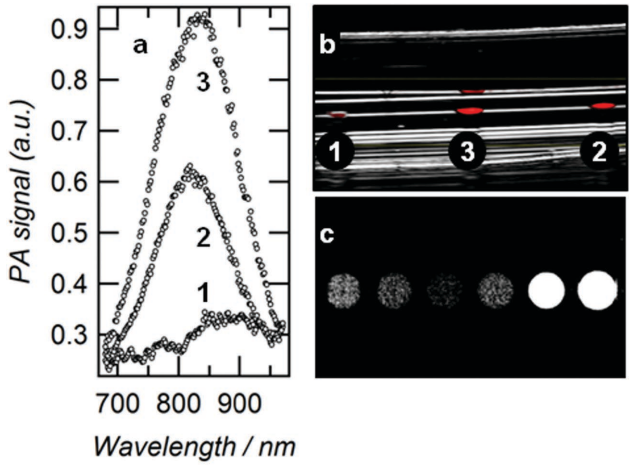

Figure 4. a) Photoacoustic spectra and b) (2.1 × 1.2) cm^2 combined B-mode ultrasound (gray) and photoacoustic (red) image at an optical wavelength of 820 nm of three microchannels that were filled with human whole blood (1), a suspension of gold nanorods in whole blood at the concentration of 1×10^{-3} M Au (2) and whole blood containing ≈3% (v/v) macrophages treated for 24 h with 400×10^{-6} M Au (3). Note that samples are not in that order in panel (b); c) CT image of a set of inclusions containing, from left to right, ≈8% (v/v) macrophagic cells treated for 24 h with 400×10^{-6} M Au, a suspension of gold nanorods at the concentration of 4×10^{-3} M Au, PBS and increasing dilutions of iodine in PBS (3.2×10^{-3}, 32×10^{-3}, and 320×10^{-3} M I).

our cells as contrast agents for a multimodal approach of biomedical imaging.

In addition to their value for biomedical imaging, another major field of application for gold nanoparticles is the photothermal ablation of cancer.[17,74–77] In this context, the same plasmonic oscillations of gold nanorods that provide for optical contrast for PAI are activated with a continuous wave in order to raise the temperature of their medium above the physiological value. Figure S5 of the Supporting Information shows that, upon excitation with a continuous wave under conditions that are harmless to blank macrophages, those treated for 24 h with 400×10^{-6} M Au undergo lethal damage within a few minutes. What is more, a monolayer of these cells is already sufficient to overheat their microenvironment above ≈65 °C (max continuous service temperature of polystyrene), as it is inferred from their effect on the Petri dish. Therefore, in addition to their value as multimodal agents of contrast for biomedical imaging, these cells hold the potential to serve as microradiators for the photothermal ablation of cancer.

3. Conclusion

In conclusion, we have disclosed a new model of gold nanorods that combine strong cationic profiles and colloidal stability, by the development of a composite shell of quaternary ammonium compounds and PEG. These particles undergo efficient and reproducible uptake from tumor-tropic cells such as macrophages, which preserve their viability and more than 90% of their innate chemotactic behavior in vitro. The amount of particles per cell is fine-tunable with the parameters of their coincubation, at least until 200 000 gold nanorods per macrophage. Under these conditions, these cells are detectible by PAI down to concentrations in the order of 1% in whole blood and by CT below 10%, which is well below the typical fraction of a leukocytic infiltrate in a tumor microenvironment. Moreover, these cells hold the potential to serve as contrast agents for the optical hyperthermia of cancer as well.

In the future, we will take the challenge to translate these results in vivo and to make a critical comparison with the conventional approach to deliver plasmonic particles to tumors, which is their PEGylation, bioconjugation[20,24,30,31] and direct infusion into the bloodstream. Indeed, while tumor-tropic cells exhibit a unique ability to cross all biological barriers before their target much better than any artificial bullet, their actual biodistribution upon modification and reinjection into a full body remains an open question. In this context, we believe that the perspective to reproduce these results with complementary kinds of tumor-tropic cells, including T cells and stem cells, represents a remarkable opportunity.

4. Experimental Section

Preparation of Polycationic Gold Nanorods: Chemicals were purchased from Sigma-Aldrich (St. Louis, MO, USA) and used as received. The preparation of polycationic gold nanorods began with the synthesis of cetrimonium-capped gold nanorods by the autocatalytic reduction of chloroauric acid with ascorbic acid, according to our variant[78] of the method by Nikoobakht and El-Sayed.[79] These particles were purified by centrifugation and transferred at a concentration of 1.8×10^{-3} M Au into a 100×10^{-3} M acetate buffer at pH 5 containing Cetyltrimethylammonium Bromide (CTAB, 500×10^{-6} M) and polysorbate 20 (50 ppm). In a typical run, an aliquot of this suspension (6 mL) was added with aqueous alpha-methoxy-omega-mercapto-PEG (MW ≈ 5000, 30 µL, 10×10^{-3} M), left to react for 30 min at 37 °C, added with MUTAB (30 µL, 100×10^{-3} M in dimethyl sulfoxide) and left at rest for another 24 h at 37 °C. Finally, these particles were purified by centrifugation and stored at a concentration of 4.5×10^{-3} M Au in sterile PBS at pH 7.4 until use.

Preparation of Plasmonic Macrophages: J774a.1 monocyte/macrophagic cells were purchased from the American Type Culture Collection (ATCC TIB-67, Manassas, VA, USA) and seeded on plastic culture dishes in Dulbecco's Modified Eagle Medium (DMEM) supplemented with fetal bovine serum (10%), L-glutamine (1%), and a penicillin–streptomycin solution (1%) (BioWhittaker, Lonza, Visp, Switzerland). Cells were kept and left to grow under standard culture conditions (37 °C, 5% CO_2).

In a typical run, an appropriate number of macrophages was cultured in complete medium for 24 h and then incubated in serum-free medium to maintain starvation. Appropriate aliquots of polycationic gold nanorods in PBS were diluted in serum-free medium, so as to achieve the final concentration of choice and left in incubation for the duration of choice.

Quantitative Measurement of Intracellular Uptake: The accumulation of gold nanorods in macrophages was quantified by an optical analysis.[24,63,64] 5×10^5 J774a.1 cells were plated in Petri dishes and treated with different concentrations of gold nanorods (4×10^{-6}, 10×10^{-6}, 40×10^{-6}, 100×10^{-6}, and 400×10^{-6} M Au) for 24 h or with 100×10^{-6} and 400×10^{-6} M Au for different durations (0.5, 1, 2, 4, 8, 16, and 24 h). Macrophages were harvested, thoroughly rinsed with PBS and fixed with paraformaldehyde (3.6% in PBS) for 10 min at room temperature. Then their pellets were washed, resuspended in PBS (120 µL), transferred into a quartz microcuvette and directed to an UV–NIR spectrophotometer (V-560, Jasco, Tokyo, Japan).

Measurement of Cellular Viability and Chemotaxis: Cellular viability was evaluated by a WST-8 assay (Cell counting kit-8, Sigma-Aldrich, St. Louis, MO, USA). The highly water-soluble tetrazolium salt WST-8

is reduced by dehydrogenases within cells, which generates the yellow product formazan. The optical absorbance of formazan at 460 nm is proportional to the number of living cells. 8×10^3 macrophages were cultured in 96-well plates and incubated with 50×10^{-6}, 100×10^{-6}, 200×10^{-6}, and 400×10^{-6} M Au for 4, 24, and 48 h. Each sample was prepared in triplicate. At the end of the treatment, each well was washed with abundant PBS and cells were incubated with serum-free medium (100 µL) supplemented with WST-8 (10%) for 2 to 4 h at 37 °C. The optical absorbance of formazan was quantified by a microplate reader (LT-400, Labtech, Bergamo, Italy) at 460 nm with a reference at 630 nm. Data were expressed as the percentage of signal with respect to controls.

A migration assay was implemented by the use of 24-well plates with polycarbonate membrane inserts (8 µm pore size, Transwell Permeable Supports, Costar, Corning Life Sciences, Lowell, MA, USA). Confluent macrophages were incubated in serum-free medium and then treated with 100×10^{-6} and 400×10^{-6} M Au for 24 h. Thereafter 2.5×10^4 cells were harvested, resuspended in serum-free medium (100 µL) and added to the upper side of the inserts. The lower well was filled with serum-free medium (600 µL) with or without MIP-1α (50 ng mL^{-1}) in the presence of bovine serum albumin (0.1%). These plates were left at 37 °C overnight. Thereafter non-migrated cells remaining on the upper side of the inserts were removed with a cotton swab. Migrated cells were fixed with paraformaldehyde (3.6% in PBS) for 10 min at room temperature and stained with Harris' hematoxylin and eosin. Each insert was observed by a light microscope at 40× magnification and migrated cells were quantified as mean ± SD in five random fields.

Photoacoustic and CT Imaging: Photoacoustic measurements were performed with a photoacoustic system from VisualSonics Inc. (Vevo LAZR, VisualSonics Inc., Toronto, Canada) that produces photoacoustic images coregistered with B-mode ultrasound images. A full description of the system is available in the work of Needles et al.[73] Photoacoustic signals were excited by a pulsed (20 Hz repetition, 6 to 8 ns pulse duration) and tunable (680 to 970 nm wavelength) Nd:YAG laser-pumped optical parametric oscillator through two rectangular fiber-optic bundles placed on both sides of a linear array transducer (13 to 24 MHz bandwidth, 23 mm × 30 mm field of view size) at an angle of 30° of the image plane. The acquisition time for a photoacoustic spectrum was about 60 s for 146 wavelength points.

A plastic device hosting six microchannels (µ-Slide VI$^{0.1}$, Ibidi GmbH, Planegg, Germany) filled with different samples was used for photoacoustic measurements (**Figure 5**a). A 5 mm layer of tissue-like material composed of polydimethylsiloxane (PDMS) mixed with TiO_2 (0.73 mg mL^{-1}) and India ink (0.25 mg mL^{-1}) was deposited onto this device in order to gain more biomedical relevance and to prevent the gold nanorods to overheat upon irradiation.[80] A full description of the tissue-like material is reported elsewhere.[81] Spectra of optical absorbance were acquired from different dilutions of gold nanorods and different formulations of plasmonic macrophages that were either dispersed in PBS or in human whole blood.

In order to acquire CT scans, we used an IRIS scanner, which is a novel multimodal preclinical tomograph for high resolution positron emission tomography/CT imaging of small animals (Raytest, Inviscan Imaging System, Strasbourg, France). The CT section is equipped with a microfocus X-ray source (35 to 80 kV voltage, 80 W power) with fixed tungsten anode and nominal maximum focal spot size of 50 µm and with a flat-panel CMOS-based X-ray detector coupled to a CsI:Tl scintillator with a thickness of 150 µm. The detector is divided into 1536 × 1944 square pixels (transaxial × longitudinal) with side length of 75 µm, for a total active surface of 115 mm × 145 mm. At full resolution, the minimum exposure time per frame in sequence mode is 39 ms, which can be shortened to 15 and 12 ms by 2 × 2 and 4 × 4 hardware rebinning, respectively. The nominal source-to-axis distance (SAD) and source-to-detector distance (SDD) are 206 and 262 mm, respectively, which results into a transaxial field of view diameter of 90 mm. Images are reconstructed by a Feldkamp-type filtered back-projection algorithm and calibrated in Hounsfield units (H.U.).

A 96-well plate containing different samples was used for CT measurements (Figure 5b). The optimization of the CT signal as a function of voltage was carried out with a clinical CT scan in the range of clinical relevance between 80 and 120 kV. Thereafter, 80 kV was chosen as the optimal voltage for CT acquisitions of samples containing gold nanorods by the IRIS scanner (80 µm voxel size, 1 mA current, 1280 n. of views, and ≈60 s acquisition time).

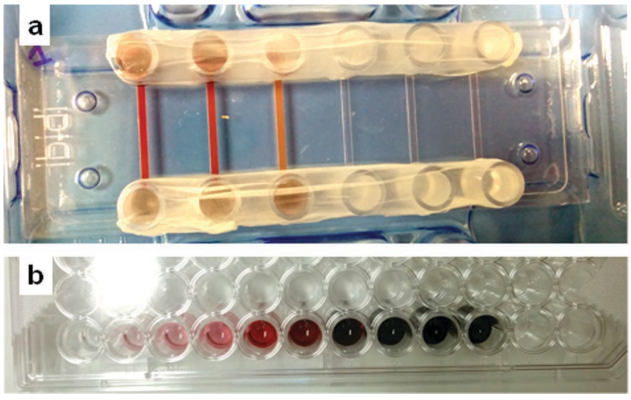

Figure 5. a) Photograph of a plastic device with three of its six microchannels filled with blood and two different dilutions of gold nanorods in blood; b) photograph of a 96-well plate filled with different dilutions of gold nanorods in PBS.

Supporting Information

Supporting Information is available from the Wiley Online Library or from the author.

Acknowledgements

This work was in part supported by the Project of Tuscan Region "NANOTREAT" and by the ERANET+ Project of Tuscan Region and European Community "LUS BUBBLE". The authors wish to thank Dr. Daniele Panetta for his expertise in X-ray microimaging.

Received: February 17, 2016
Revised: April 21, 2016
Published online:

[1] X. Yang, M. Yang, B. Pang, M. Vara, Y. Xia, *Chem. Rev.* **2015**, *115*, 10410.
[2] C. C. Bao, N. Beziere, P. del Pino, B. Pelaz, G. Estrada, F. R. Tian, V. Ntziachristos, J. M. de la Fuente, D. X. Cui, *Small* **2013**, *9*, 68.
[3] E. C. Dreaden, A. M. Alkilany, X. H. Huang, C. J. Murphy, M. A. El-Sayed, *Chem. Soc. Rev.* **2012**, *41*, 2740.
[4] L. C. Kennedy, L. R. Bickford, N. A. Lewinski, A. J. Coughlin, Y. Hu, E. S. Day, J. L. West, R. A. Drezek, *Small* **2011**, *17*, 169.
[5] F. Ratto, P. Matteini, S. Centi, F. Rossi, R. Pini, *J. Biophotonics* **2011**, *4*, 64.
[6] J. Y. Chen, M. X. Yang, Q. A. Zhang, E. C. Cho, C. M. Cobley, C. Kim, C. Glaus, L. H. V. Wang, M. J. Welch, Y. N. Xia, *Adv. Funct. Mater.* **2010**, *20*, 3684.
[7] P. J. van den Berg, K. Daoudi, W. Steenbergen, *Photoacoustics* **2015**, *3*, 89.
[8] L. V. Wang, *Nat. Photonics* **2009**, *3*, 503.
[9] A. M. Alkilany, L. B. Thompson, S. P. Boulos, P. N. Sisco, C. J. Murphy, *Adv. Drug Delivery Rev.* **2012**, *64*, 190.

[10] N. Khlebtsov, L. Dykman, *Chem. Soc. Rev.* **2011**, *40*, 1647.
[11] N. Lewinski, V. Colvin, R. Drezek, *Small* **2008**, *4*, 26.
[12] P. K. Jain, K. S. Lee, I. H. El-Sayed, M. A. El-Sayed, *J. Phys. Chem. B* **2006**, *110*, 7238.
[13] H. J. Chen, L. Shao, Q. Li, J. F. Wang, *Chem. Soc. Rev.* **2013**, *42*, 2679.
[14] L. Vigderman, B. P. Khanal, E. R. Zubarev, *Adv. Mater.* **2012**, *36*, 4811.
[15] J. Perez-Juste, I. Pastoriza-Santos, L. M. Liz-Marzan, P. Mulvaney, *Coord. Chem. Rev.* **2005**, *249*, 1870.
[16] S. Kessentini, D. Barchiesi, *Biomed. Opt. Express* **2012**, *3*, 590.
[17] G. von Maltzahn, J. H. Park, A. Agrawal, N. K. Bandaru, S. K. Das, M. J. Sailor, S. N. Bhatia, *Cancer Res.* **2009**, *69*, 3892.
[18] M. Mazzoni, F. Ratto, C. Fortunato, S. Centi, F. Tatini, R. Pini, *J. Phys. Chem. C* **2014**, *118*, 20018.
[19] P. P. Joshi, S. J. Yoon, Y. S. Chen, S. Emelianov, K. V. Sokolov, *Biomed. Opt. Express* **2013**, *4*, 2609.
[20] C. Ungureanu, R. Kroes, W. Petersen, T. A. M. Groothuis, F. Ungureanu, H. Janssen, F. W. B. van Leeuwen, R. P. H. Kooyman, S. Manohar, T. G. van Leeuwen, *Nano Lett.* **2011**, *11*, 1887.
[21] J. V. Jokerst, M. Thangaraj, P. J. Kempen, R. Sinclair, S. S. Gambhir, *ACS Nano* **2012**, *6*, 5920.
[22] Y. Huang, F. Rosei, F. Vetrone, *Nanoscale* **2015**, *7*, 5178.
[23] G. Terentyuk, E. Panfilova, V. Khanadeev, D. Chumakov, E. Genina, A. Bashkatov, V. Tuchin, A. Bucharskaya, G. Maslyakova, N. Khlebtsov, B. Khlebtsov, *Nano Res.* **2014**, *7*, 325.
[24] F. Ratto, E. Witort, F. Tatini, S. Centi, L. Lazzeri, F. Carta, M. Lulli, D. Vullo, F. Fusi, C. T. Supuran, A. Scozzafava, S. Capaccioli, R. Pini, *Adv. Funct. Mater.* **2015**, *25*, 316.
[25] F. Tatini, I. Landini, F. Scaletti, L. Massai, S. Centi, F. Ratto, S. Nobili, G. Romano, F. Fusi, L. Messori, E. Mini, R. Pini, *J. Mater. Chem. B* **2014**, *2*, 6072.
[26] T. Niidome, M. Yamagata, Y. Okamoto, Y. Akiyama, H. Takahashi, T. Kawano, Y. Katayama, Y. Niidome, *J. Controlled Release* **2006**, *114*, 343.
[27] X. H. Huang, X. H. Peng, Y. Q. Wang, Y. X. Wang, D. M. Shin, M. A. El-Sayed, S. M. Nie, *ACS Nano* **2010**, *4*, 5887.
[28] Y. Akiyama, T. Mori, Y. Katayama, T. Niidome, *J. Controlled Release* **2009**, *139*, 81.
[29] S. D. Perrault, C. Walkey, T. Jennings, H. C. Fischer, W. C. W. Chan, *Nano Lett.* **2009**, *9*, 1909.
[30] S. Centi, F. Tatini, F. Ratto, A. Gnerucci, R. Mercatelli, G. Romano, I. Landini, S. Nobili, A. Ravalli, G. Marrazza, E. Mini, F. Fusi, R. Pini, *J. Nanobiotechnol.* **2014**, *12*, 55.
[31] B. C. Rostro-Kohanloo, L. R. Bickford, C. M. Payne, E. S. Day, L. J. Anderson, M. Zhong, S. Lee, K. M. Mayer, T. Zal, L. Adam, C. P. Dinney, R. A. Drezek, J. L. West, J. H. Hafner, *Nanotechnology* **2009**, *20*, 434005.
[32] C. Ayala-Orozco, C. Urban, M. W. Knight, A. S. Urban, O. Neumann, S. W. Bishnoi, S. Mukherjee, A. M. Goodman, H. Charron, T. Mitchell, M. Shea, R. Roy, S. Nanda, R. Schiff, N. J. Halas, A. Joshi, *ACS Nano* **2014**, *6*, 6372.
[33] P. Puvanakrishnan, J. Park, D. Chatterjee, S. Krishnan, J. W. Tunnell, *Int. J. Nanomed.* **2012**, *7*, 1251.
[34] S. K. Sriraman, B. Aryasomayajula, V. P. Torchilin, *Tissue Barriers* **2014**, *2*, e29528.
[35] A. J. Trinidad, S. J. Hong, Q. Peng, S. J. Madsen, H. Hirschberg, *Lasers Surg. Med.* **2014**, *46*, 310.
[36] M. R. Choi, R. Bardhan, K. J. Stanton-Maxey, S. Badve, H. Nakshatri, K. M. Stantz, N. Cao, N. J. Halas, S. E. Clare, *Cancer Nano* **2012**, *3*, 47.
[37] T. D. Yang, W. Choi, T. H. Yoon, K. J. Lee, J. S. Lee, S. H. Han, M. G. Lee, H. S. Yim, K. M. Choi, M. W. Park, *J. Biomed. Opt.* **2012**, *17*, 128003.
[38] S. J. Madsen, S. K. Baek, A. R. Makkouk, T. Krasieva, H. Hirschberg, *Ann. Biomed. Eng.* **2012**, *40*, 507.
[39] M. R. Choi, K. J. Stanton-Maxey, J. K. Stanley, C. S. Levin, R. Bardhan, D. Akin, S. Badve, J. Sturgis, J. P. Robinson, R. Bashir, N. J. Halas, S. E. Clare, *Nano Lett.* **2007**, *7*, 3759.
[40] L. C. Kennedy, A. S. Bear, J. K. Young, N. A. Lewinski, J. Kim, A. E. Foster, R. A. Drezek, *Nanoscale Res. Lett.* **2011**, *6*, 283.
[41] L. Pascucci, V. Coccè, A. Bonomi, D. Ami, P. Ceccarelli, E. Ciusani, L. Viganò, A. Locatelli, F. Sisto, S. M. Doglia, E. Parati, M. E. Bernardo, M. Muraca, G. Alessandri, G. Bondiolotti, A. Pessina, *J. Controlled Release* **2014**, *192*, 262.
[42] J. Zhao, J. Vykoukal, M. Abdelsalam, A. Recio-Boiles, Q. Huang, Y. Qiao, B. Singhana, M. Wallace, R. Avritscher, M. P. Melancon, *Nanotechnology* **2014**, *25*, 405101.
[43] L. Li, Y. Guan, H. Liu, N. Hao, T. Liu, X. Meng, C. Fu, Y. Li, Q. Qu, Y. Zhang, S. Ji, L. Chen, D. Chen, F. Tang, *ACS Nano* **2011**, *5*, 7462.
[44] R. Mooney, L. Roma, D. Zhao, D. Van Haute, E. Garcia, S. U. Kim, A. J. Annala, K. S. Aboody, J. M. Berlin, *ACS Nano* **2014**, *8*, 12450.
[45] K. Schnarr, R. Mooney, Y. Weng, D. Zhao, E. Garcia, B. Armstrong, A. J. Annala, S. U. Kim, K. S. Aboody, J. M. Berlin, *Adv. Healthcare Mater.* **2013**, *2*, 976.
[46] S. Tan, T. Wu, D. Zhang, Z. Zhang, *Theranostics* **2015**, *5*, 863.
[47] R. Noy, J. W. Pollard, *Immunity* **2014**, *41*, 49.
[48] P. Barcellos-de-Souza, V. Gori, F. Bambi, P. Chiarugi, *Biochim. Biophys. Acta* **2013**, *1836*, 321.
[49] P. Chiarugi, *Oncoimmunology* **2013**, *2*, e25563.
[50] A. Mantovani, P. Allavena, *J. Exp. Med.* **2015**, *212*, 435.
[51] R. Weissleder, M. Nahrendorf, M. J. Pittet, *Nat. Mater.* **2014**, *13*, 125.
[52] J. B. Mitchem, D. J. Brennan, B. L. Knolhoff, B. A. Belt, Y. Zhu, D. E. Sanford, L. Belaygorod, D. Carpenter, L. Collins, D. Piwnica-Worms, S. Hewitt, G. M. Udupi, W. M. Gallagher, C. Wegner, B. L. West, A. Wang-Gillam, P. Goedegebuure, D. C. Linehan, D. G. DeNardo, *Cancer Res.* **2013**, *73*, 1128.
[53] R. Z. Panni, D. C. Linehan, D. G. DeNardo, *Immunotherapy* **2013**, *5*, 1075.
[54] B. Wang, E. Yantsen, T. Larson, A. B. Karpiouk, S. Sethuraman, J. L. Su, K. Sokolov, S. Y. Emelianov, *Nano Lett.* **2009**, *9*, 2212.
[55] C. E. Lewis, R. Leek, A. Harris, J. O. McGee, *J. Leukoc. Biol.* **1995**, *57*, 747.
[56] C. O'Sullivan, C. E. Lewis, *J. Pathol.* **1994**, *172*, 229.
[57] D. A. Loeffler, P. C. Keng, R. B. Baggs, E. M. Lord, *Int. J. Cancer* **1990**, *45*, 462.
[58] L. Vigderman, P. Manna, E. R. Zubarev, *Angew. Chem. Int. Ed.* **2012**, *51*, 636.
[59] T. S. Hauck, A. A. Ghazani, W. C. W. Chan, *Small* **2008**, *4*, 153.
[60] E. Oh, J. B. Delehanty, K. E. Sapsford, K. Susumu, R. Goswami, J. B. Blanco-Canosa, P. E. Dawson, J. Granek, M. Shoff, Q. Zhang, P. L. Goering, A. Huston, I. L. Medintz, *ACS Nano* **2011**, *5*, 6434.
[61] J. B. Delehanty, K. Boeneman, C. E. Bradburne, K. Robertson, J. E. Bongard, I. L. Medintz, *Ther. Delivery* **2010**, *1*, 411.
[62] H. Yuan, A. M. Fales, T. Vo-Dinh, *J. Am. Chem. Soc.* **2012**, *134*, 11358.
[63] P. Matteini, F. Ratto, F. Rossi, M. de Angelis, L. Cavigli, R. Pini, *J. Biophotonics* **2012**, *5*, 868.
[64] F. Ratto, P. Matteini, A. Cini, S. Centi, F. Rossi, F. Fusi, R. Pini, *J. Nanopart. Res.* **2011**, *13*, 4337.
[65] P. G. Etchegoin, E. C. Le Ru, M. Meyer, *J. Chem. Phys.* **2006**, *125*, 164705.
[66] P. Menten, A. Wuyts, J. Van Damme, *Cytok. Growth Factor Rev.* **2002**, *13*, 455.
[67] E. I. Galanzha, D. A. Nedosekin, M. Sarimollaoglu, A. I. Orza, A. S. Biris, V. V. Verkhusha, V. P. Zharov, *J. Biophotonics* **2015**, *8*, 81.
[68] V. P. Zharov, *Nat. Photonics* **2011**, *5*, 110.
[69] H. Ju, R. A. Roy, T. W. Murray, *Biomed. Opt. Express* **2012**, *4*, 66.
[70] E. Y. Lukianova-Hleb, X. Y. Ren, R. R. Sawant, X. W. Wu, V. P. Torchilin, D. O. Lapotko, *Nat. Med.* **2014**, *20*, 778.

[71] E. Lukianova-Hleb, Y. Hu, L. Latterini, L. Tarpani, S. Lee, R. A. Drezek, J. H. Hafner, D. O. Lapotko, *Nano Lett.* **2010**, *4*, 2109.
[72] R. K. Saha, M. C. Kolios, *J. Biomed. Opt.* **2011**, *16*, 115003.
[73] A. Needles, A. Heinmiller, P. Ephrat, C. Bilan-Tracey, A. Trujillo, C. Theodoropoulos, D. Hirson, F. S. Foster, *IEEE Int. Ultrason. Symp. Proc.* **2010**, 390.
[74] C. Iodice, A. Cervadoro, A. Palange, J. Key, S. Aryal, M. R. Ramirez, C. Mattu, G. Ciardelli, B. E. O'Neill, P. Decuzzi, *Opt. Laser Eng.* **2016**, *76*, 74.
[75] Z. W. Li, S. N. Yin, L. Cheng, K. Yang, Y. G. Li, Z. Liu, *Adv. Funct. Mater.* **2014**, *24*, 2312.
[76] X. H. Huang, P. K. Jain, I. H. El-Sayed, M. A. El-Sayed, *Lasers Med. Sci.* **2008**, *23*, 217.
[77] B. Khlebtsov, V. Zharov, A. Melnikov, V. Tuchin, N. Khlebtsov, *Nanotechnology* **2006**, *17*, 5167.
[78] F. Ratto, P. Matteini, F. Rossi, R. Pini, *J. Nanopart. Res.* **2009**, *12*, 2029.
[79] B. Nikoobakht, M. A. El-Sayed, *Chem. Mater.* **2003**, *15*, 1957.
[80] L. Cavigli, M. de Angelis, F. Ratto, P. Matteini, F. Rossi, S. Centi, F. Fusi, R. Pini, *J. Phys. Chem. C* **2014**, *118*, 16140.
[81] C. Avigo, N. Di Lascio, P. Armanetti, C. Kusmic, L. Cavigli, F. Ratto, S. Meucci, C. Masciullo, M. Cecchini, R. Pini, F. Faita, L. Menichetti, *J. Biomed. Opt.* **2015**, *20*, 46008.